energies

MDPI

Article

A Sizing Method for PV–Battery–Generator Systems for Off-Grid Applications Based on the LCOE

Ioannis E. Kosmadakis and Costas Elmasides *

Department of Environmental Engineering, Democritus University of Thrace, 67100 Xanthi, Greece; ikosmada@env.duth.gr
* Correspondence: kelmasid@env.duth.gr; Tel.: +30-25410-79876

Abstract: Electricity supply in nonelectrified areas can be covered by distributed renewable energy systems. The main disadvantage of these systems is the intermittent and often unpredictable nature of renewable energy sources. Moreover, the temporal distribution of renewable energy may not match that of energy demand. Systems that combine photovoltaic modules with electrical energy storage (EES) can eliminate the above disadvantages. However, the adoption of such solutions is often financially prohibitive. Therefore, all parameters that lead to a functionally reliable and self-sufficient power generation system should be carefully considered during the design phase of such systems. This study proposes a sizing method for off-grid electrification systems consisting of photovoltaics (PV), batteries, and a diesel generator set. The method is based on the optimal number of PV panels and battery energy capacity whilst minimizing the levelized cost of electricity (LCOE) for a period of 25 years. Validations against a synthesized load profile produced grid-independent systems backed by different accumulator technologies, with LCOEs ranging from 0.34 EUR/kWh to 0.46 EUR/kWh. The applied algorithm emphasizes a parameter of useful energy as a key output parameter for which the solar harvest is maximized in parallel with the minimization of the LCOE.

Keywords: photovoltaics; battery; diesel generator; sizing method; renewable energy sources; off-grid power systems; levelized cost of electricity; distributed energy resources; electrical energy storage

Citation: Kosmadakis, I.E.; Elmasides, C. A Sizing Method for PV–Battery–Generator Systems for Off-Grid Applications Based on the LCOE. *Energies* **2021**, *14*, 1988. https://doi.org/10.3390/en14071988

Academic Editor: Praveen Cheekatamarla

Received: 9 March 2021
Accepted: 1 April 2021
Published: 3 April 2021

1. Introduction

Renewable energy sources can, in the long term, ensure a sustainable energy supply and reduce local and global air pollutant emissions. In addition, it is the most promising solution for supplying electrical load to remote and rural areas that are not served by an electrical grid. According to a recent study [1], the population without access to electricity was estimated to be 861 million in 2018. Moreover, in the same study, it was also mentioned that, in 2018, about 2.65 billion people were living without access to clean cooking, which means that they did not have access to fuels and technologies such as natural gas, liquefied petroleum gas (LPG), electricity, and biogas.

Reducing the cost of photovoltaics while increasing their efficiency has made off-grid solar systems more economically attractive, resulting in increased use of these systems to meet the energy needs of the abovementioned populations. Specifically, since 2010, more than 180 million off-grid solar systems have been installed in these kinds of applications. However, only 17% of these systems were used to meet household needs, whereas the peak power (up to 10 W) of the other 83% was mainly used for lighting and charging mobiles [1]. In order to further increase the number of systems that meet household needs while improving the quality of these people's lives, methods should be developed which lead to optimum techno-economic solutions. Some of the efforts that have been made in this direction are described below.

Several research teams dealt with optimal dimensioning of PV–battery systems using appropriate software tools. For example, a widely used software is the Hybrid Optimization

Model for Electric Renewables (HOMER) developed in order to determine the optimal size of system components by carrying out techno-economic analysis. In El-Houari et al. [2], real monthly electrical demands and hourly site-specific meteorological conditions were used to calculate, via HOMER Pro software, the PV and battery requirements for rural African regions. A very comprehensive review [3] describes how this software works. Input data including meteorological data, load profile, equipment characteristics, and economic and technical data are required for simulation and optimization. Optimization occurs by finding an optimal value for an objective function which is the present value of the sum of costs minus the sum of revenues. The final step concerns the sensitivity analysis where an evaluation of the variation in uncertain parameters (such as fuel cost, wind speed, solar radiation, electricity price, and component cost) on optimal sizing takes place.

Other available software tools for optimal sizing of standalone PV–battery systems are Improved Hybrid Optimization by Genetic Algorithms (IHOGA), Transient Systems Simulation Program (TRNSYS), RETScreen, and PVSYST [4]. All of these programs use almost the same input data as those reported for HOMER in the previous paragraph. However, the results of each software and their application differ, as described in detail in [4].

In addition to software, many research groups developed optimization tools and techniques to approach an optimum techno-economic solution. These attempts can be classified into various categories: genetic algorithms, particle swarm optimization (PSO), simulated annealing, and ant colony algorithm. Information on the development philosophy of these methods and how to use them can be found in a previous review [5]. In their work, Dufo-López et al. [6] studied the multi-objective design of PV–wind–diesel configurations coupled with electrical energy storage (EES) in order to minimize both the levelized cost of electricity (LCOE) and CO_2 emissions, employing relatively fast evolutionary algorithms. Results showed that the best pareto fronts included a diesel generator that contributes to the overall economic and environmental performance. In Maleki et al. [7], a combinatorial optimization method based on the harmony search algorithm for sizing off-grid PV–battery and generator systems was presented. In this study, the proposed method outperformed a simulated annealing method, displaying extremely fast runtimes, although battery technology and various battery specifics such as depth of discharge and cycle life were not considered. Simulated annealing genetic algorithms were employed by Wei et al. [8] to optimize coal-fired boiler operation so as to reduce NOx emissions, thereby exhibiting accurate solutions in a low computing time. Similarly, in [9], Ghafoor et al. presented a deterministic and straightforward off-grid PV–battery configuration model for a residential case study in Pakistan accompanied by a lifecycle cost analysis without considering battery technology.

In [10], Mandelli et al. proposed an off-grid PV–battery sizing method for rural areas of developing countries introducing the loss of load probability and the electricity unit cost as key aspects in the sizing process. In a case study, they displayed the effectiveness of their numerical method and showed that accurate results are required in order to optimize the energy and economic cost of the system. Furthermore, in [11], Mandelli et al. investigated the impact of load profile uncertainty on PV and battery sizing and introduced an algorithm for implementing stochastic load profile formulation.

In a paper by Shank et al. [12], a dispatch-coupled sizing method based on a PSO-enabled algorithm for batteries in systems with different penetration levels of renewables was introduced. Results showed that their metaheuristic modifications of the particle swarm optimization avoided premature convergence to local optima and was effective in large-scale energy systems with different penetration levels of RES. Moreover, in [13], Rodríguez-Gallegos et al. employed a multi-objective optimization approach, considering the LCOE, CO_2 emissions, and grid voltage for sizing interconnected PV–battery–diesel combinations.

Recently, Li [14] studied the PV–battery optimization problem of grid-connected households by incorporating load demand uncertainty and time-of-use tariffs into a siz-

ing genetic algorithm involving a time-series simulation, showing more realistic results compared to algorithms using average data from chosen sites. Reinforcement learning and evolutionary algorithms have an extended scope and have also been reported to be effective in various applications such as battery-related energy management systems and electrical vehicles [15,16].

A common feature of sizing methods is the construction of an objective function and the attempt to optimize it through changes in operational, technical, and economic parameters. The most widely used objective function is the LCOE [10,17,18]. The LCOE provides an indication of the cost per unit of energy throughout the operation of the sizing system. In general, LCOE aggregates all costs over the lifetime of an energy system and divides them by the total energy production over the lifetime.

In this work, we propose a design method for non-interconnected photovoltaic systems with batteries and generator sets (PVBG). This method is based on the synthesis of the objective function expressed by the LCOE. Its aim is the selection of an effective combination of PV panel quantity and nominal energy capacity of the battery, so that the cost of the system per unit of energy for a period of 25 years is minimized. The sizing method considers a detailed electricity demand profile; therefore, the optimized PVBG configuration matches with the energy consumption more realistically, in contrast to algorithms using average data from specific sites. Additionally, this enumerative method not only produces optimal PVBG configurations but also determines the actually utilized solar energy harvest, thereby calculating a more precise LCOE.

After this introduction, the off-grid design of a PVBG system is discussed in Section 2. In this section, the hourly PV power output is estimated and linked to a typical household load profile. The operation and sizing algorithms of the PVBG system, as well as the system cost analysis based on the LCOE, are presented and described in detail. The results of the applied sizing method are validated and presented in Section 3, followed by a discussion in Section 4. Concluding remarks and suggestions for future work are given in the last section.

2. Materials and Methods

2.1. Off-Grid PV–Battery–Generator System

Distributed energy resources (DERs) such as PV modules, power electronics, and batteries can be integrated into a unified and autonomous electrification system in several ways. A key consideration when planning PV–battery systems is the selection of the alternating current (AC) or direct current (DC) system architecture, i.e., the preference among AC or DC bus utilization, which differs in power converter arrangements and conversion steps. Along with the electrical energy generation and storage, an auxiliary power source in the form of a generator has to be added to the system to achieve total grid independence.

In this section, the sizing method for PV–battery–generator systems oriented towards off-grid applications is presented in detail. The key points of the method are depicted in Figure 1.

2.1.1. Preference of the DC-Coupled Architecture

In DC-coupled systems, the PV arrays are connected to the DC busbars via unidirectional DC/DC converters, commonly known as maximum power point tracking (MPPT) solar charge controllers. The battery is directly connected to the DC busbars, forming together with the PV output a parallel connection to the DC side of an inverter, as shown in Figure 2.

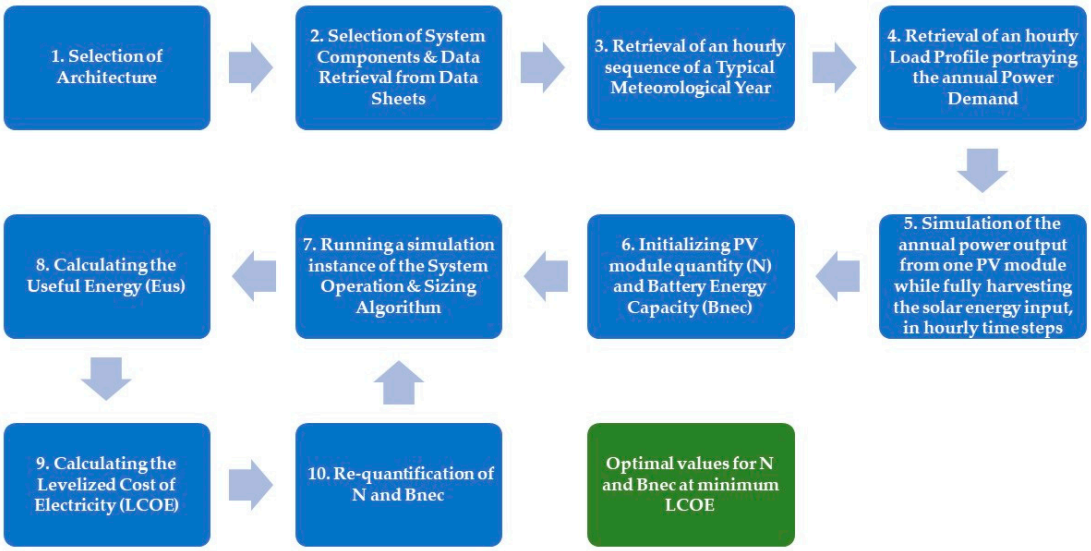

Figure 1. Flow diagram depicting the basic steps of the proposed photovoltaic (PV)–battery sizing method. Steps 7 to 10 are iterated for a specified range of PV modules and battery energy capacities, subsequently highlighting optimal values for *N* and Bnec at minimum levelized cost of electricity (LCOE).

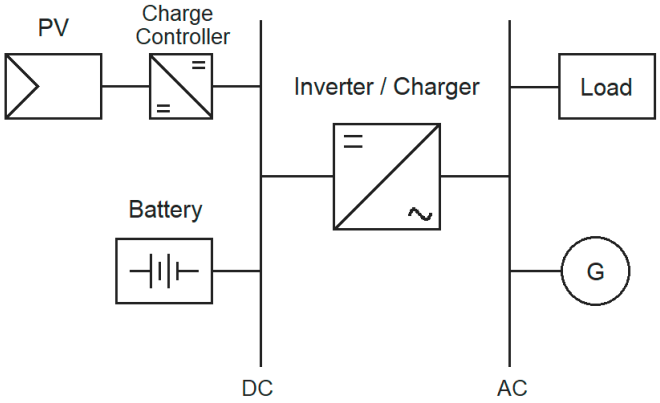

Figure 2. Off-grid system architecture of direct current (DC)-coupled PV–battery–generator system.

In this setup, the PV modules power the load on the consumption side through the DC/DC converter and then through a DC/AC inverter. PV power also charges the battery through the DC/DC converter in a single conversion step, and the discharging battery power also contributes to load supply via the DC/AC inverter. In off-grid systems, a standby power source on the AC side of the inverter can act as a backup for energy shortages and supply power directly to the load. Battery charging by the standby power source occurs through an additional AC/DC rectifier, usually, a charger incorporated into the inverter, as shown in Figure 2.

In AC-coupled systems, the typical AC bus is used as the conductive medium linking the power source, energy storage, and load. The PV arrays and the battery are connected to the AC bus via unidirectional and bidirectional DC/AC inverters, respectively. Since, in this setup, the load is directly connected to the AC bus, the power supply of the load is done from the PV modules and the discharging battery in a single conversion step. Again, in off-grid systems, the standby power source supplies power directly to the load when needed.

For the most part, off-grid PVBG systems on a smaller scale follow a DC-coupled system architecture, primarily for practical reasons, since electrochemical accumulators work with DC. This simple and robust setup facilitates the reliable and efficient charging of batteries, especially in instances where the surplus renewable energy harvest needs to be

maximized. Another critical issue is the fact that, when batteries are too far discharged, a battery inverter shuts down the AC output to protect the battery from damage. In the case of a DC architecture, this is relatively inconsequential as solar energy eventually recharges the battery through the charge controller. On the contrary, when batteries are too far discharged in an AC architecture, special use of a backup generator is required to provide power references, such as voltage and frequency, to allow renewable solar and battery inverters to reconnect.

Furthermore, DC-coupled setups are very cost-effective for small to medium-size off-grid systems. Solar charge controllers are highly modular and scalable, i.e., additional PV arrays can be easily added to the DC bus, if required, using comparatively low-cost solar charge controllers. Consequently, for these reasons, a DC architecture was preferred for simulation in this work.

2.1.2. Selection of the System Components

The decisive criteria for the selection of PV panels are the degree of efficiency as a function of the module temperature coefficients, the product and performance module warranties, and the purchasing cost of PV in EUR per installed capacity. In the present work, only photovoltaic modules from crystalline silicon were considered since they are the most prevalent PV type in the PV market.

Industrially produced crystalline silicon PV cells currently achieve efficiencies ranging from 18% to 22% under standard test conditions (STCs) [19]. The industry average of solar panel manufacturer warranties varies from 10 to 25 years. Considering the global declining trend in module average selling price, the reported average crystalline silicon module prices in 2020 ranged from approximately 0.40 EUR/Wp to 0.25 EUR/Wp [20].

For the simulation purposes of the present work, the module selected was SolarCall SCM310, a passivated emitter and rear contact (PERC) PV module made of monocrystalline silicon, from a European manufacturer [21]. The module's installed capacity is 310 Wp with a surface area of 1.627 m^2, resulting in a module energy efficiency of approximately 19%, under STCs. According to the manufacturer's datasheet, the peak power temperature coefficient is $-0.40\%/^{\circ}C$. The manufacturer product and linear power warranties are 15 years and 30 years, respectively. More specifically, the performance warranty for 15 years is 91.2% and that for 30 years is 80.6% of rated power. Cost of the module was inquired online, and offers ranging from 0.45 EUR/Wp to 0.35 EUR/Wp were collected from selected distributors.

For the power electronics simulation requirements, features were taken from data sheets of established power electronics manufacturers. More specifically, in every simulation run, the energy flows originating from a PV array block were handled by an MPPT solar charge controller, and its efficiency level was considered relatively stable throughout the whole power range (approximately 95%). Nevertheless, efficiency estimations of inverters are more complicated since inverter efficiency is a function of apparent power output. Inverters are generally designed to achieve a high power factor when operating at full power. Actual conditions vary, however. Therefore, the power factor of the inverters used in the simulations was considered greater than 90% when the power output was greater than 20% of the nominal inverter power [22].

The solar charge controllers and the battery inverters considered for simulation in this work were from Victron Energy. The charge controllers exhibit a PV input voltage, ranging from 75 V to 150 V and a current output up to 70 A. The inverters supply up to 5000 VA apparent power and also feature a battery charger and generator triggering. The battery charging current and automatic generator triggering can be programmed with a computer. Although manufacturer product warranties are limited to 5 years, the power converters are expected to last 25 years. Costs of the specific items were inquired online, and offers were collected from selected distributors, which were 20% lower than the official prices published quarterly by established manufacturers [23].

In self-sufficient power systems, the EES is heavily used to facilitate power deficits from RES and to operate as a short-term storage medium. In recent years, lithium-ion batteries have surged in popularity and overtaken lead–acid batteries as the preferred EES medium [24]. Nevertheless, in many instances, the lead–acid battery is still the first choice when it comes to EES, especially when the initial capital cost is a critical point of consideration [25]. Another point of consideration in the EES selection process is the end-of-life management of the anode and cathode material of the accumulators. In contrast to the lithium-ion battery, the lead–acid battery exhibits a very high recovery rate [26]. Furthermore, lithium-ion batteries must operate in a strictly defined voltage and temperature window. Safe and efficient charging and discharging of lithium-ion accumulators is assured only through the use of a battery management system (BMS), which again increases cost.

Consequently, both battery types were studied in this work and simulated as an EES resource. Complying with the DC-coupled architecture, the battery was directly connected to the DC busbars and, therefore, defined the system voltage. Commonly, higher power levels require greater system voltage, since delivering more power at a given voltage takes more current, which in turn leads to higher power losses. Here, the considered nominal system voltage was 48 V for both battery types. Equally important is the nominal battery capacity since the product of voltage and capacity defines the nominal energy capacity of the battery used in the simulation. Furthermore, significant battery features such as nominal battery cycles at maximum depth of discharge (DOD) and calendar battery life were extracted from datasheets of renowned battery manufacturers. More specifically, in this study, the lead–acid battery selected was the RES SOPzV from Systems Sunlight S.A. [27] and the lithium-ion battery selected was the LFP-Smart from Victron Energy [28], both labelled as EES solutions used in conjunction with RES. Both batteries were sized at approximately 5 kWh energy capacity intervals, and, according to the manufacturers, the cycle life at 50% DOD was 2500 cycles for the lead–acid battery and 5000 cycles for the lithium-ion battery. Moreover, different theoretical maximum calendar lives of 5 years and 10 years, respectively, were included in the simulation, in line with [29,30]. The cost per kWh for each battery type was inquired online, and offers ranging from 154 EUR/kWh to 574 EUR/kWh, for lead–acid and lithium-ion batteries, respectively, were collected from selected distributors.

Generator sets are fuel power systems comprising an engine and an alternator and are broadly categorized into primary and standby generators. The latter are used as backup generators (BGs) that instantly supply power to the load when the primary power supply, in this work the PV–battery system, fails. Optimal sizing of diesel generator sets in hybrid energy systems is an essential step in planning economical off-grid electrification systems [31], with resiliency being a key aspect to consider [32]. Currently, natural gas- and diesel-powered engines are the industry standard, although biomass and biogas are gaining ground. Nevertheless, there are several other crucial factors to consider before choosing a BG. These systems run, to a high degree, infrequently and remain in a cold state for most of their cycle life. Therefore, it is important to carefully define the required function and the operating time intervals of BGs in an off-grid system. The sizing procedure for BGs must take into account the maximum continuous time use (CTU), the estimated annual operation time (APT), and the average load value (ALV) during BG operation as a function of the rated generator power. Furthermore, the amount of electricity supplied to the load by the BG depends on the quantity of fuels consumed, which in turn is a function of generator efficiency and operation time. The total operational lifespan of such systems can reach 20 years [33] as long as the generator is well maintained and CTU and APT are not exceeded.

Once again generator specifications were taken from manufacturer datasheets and used to simulate standby BG operation on an hourly basis, corresponding to PV, battery, and power converter components. The considered generator in this study was the Hyundai DHY6000SE diesel standby generator, capable of supplying up to 4.5 kW of power over

a single phase, with maximum CTU and APT values limited to 5 and 500 h, respectively. The standard warranty for this product is 2 years, yet the manufacturer claims that a total lifespan of above 10,000 h can be achieved with correct maintenance and operation (that is, if the average load is not lower than 30% or higher than 80% of the rated generator output). The capital cost for this generator set varies from 1390 EUR to 1500 EUR per item depending on location and shipping. Annual operation and maintenance cost estimations range from 235 to 260 EUR.

2.2. Annual Electricity Generation Estimation

A method for accurately estimating the annual energy winnings from PV systems was examined in previous work [25,34] in more detail. In summary, simulating the annual PV energy output requires the use of the PV datasheet and hourly sequenced meteorological data for a specified position. Time series on an hourly basis of global horizontal irradiance (GHI), onsite atmospheric temperature (T), and horizontal windspeed (WS) are used for at least one calendar year to produce analogous sequences of direct normal irradiance (DNI) and diffuse horizontal irradiance (DHI). This was done using the DISC model from [35,36]. Given the PV surface and PV azimuth angles, sequences of the solar angle incidence (AOI) as a function of solar position with respect to latitude, longitude, and altitude were calculated. An acceptable albedo of 0.25 was used for all sizing simulations in this study and, lastly, hourly sequences of the total solar irradiance instance (Epoa) hitting the PV modules were calculated. The above-simulated sequences were fed at first into the Sandia Cell and Module Temperature Model [37], to compute PV cell (TC) and PV module temperatures (TM), and subsequently into the five-parameter model [38] leading to the five corresponding outputs of the model: (i) the photocurrent (IL), (ii) the diode reverse saturation current (I0), (iii) the series resistance (Rs), (iv) the shunt resistance (Rsh), and (v) the modified diode ideality factor (nNsVth). These outputs comprise the inputs for the widely accepted single-diode model [39,40] for photovoltaic modules from which power estimations are obtained.

Losses because of PV module reflectivity and soiling were taken into consideration. According to PV manufacturers, PV modules are typically guaranteed to deliver 80% of the rated power output at the end of their lifetime. Hence, the annual PV energy output was corrected further with a degradation factor of 0.9, optimizing mean power output estimations over a typical 25 year period. Model implementation and data processing were done in Python using the PVLIB solar simulation library for PV energy systems [41–45].

Using a typical meteorological year (TMY) [46] for a specified location (Xanthi, Greece) in conjunction with the above-described electricity generation estimation method, a total of 8760 hourly sequenced data points were generated, representing the annual electrical energy output from one PV module. This referential output was then multiplied by the number of PV modules used in each sizing step to determine the total annual energy winnings from a certain PV capacity instance of the algorithm.

2.3. Reference Load Profile

A consumer load profile of an average four-person household was synthesized by approximating the electrical appliance usage over a whole year, which was then used as a reference for the sizing algorithm developed in this study. The load profile was scaled to the annual electricity consumption of approximately 5500 kWh with the winter months (in the northern hemisphere) from December to February acting as the baseload months with a baseload of approximately 300 kWh, as one can observe in Figure 3.

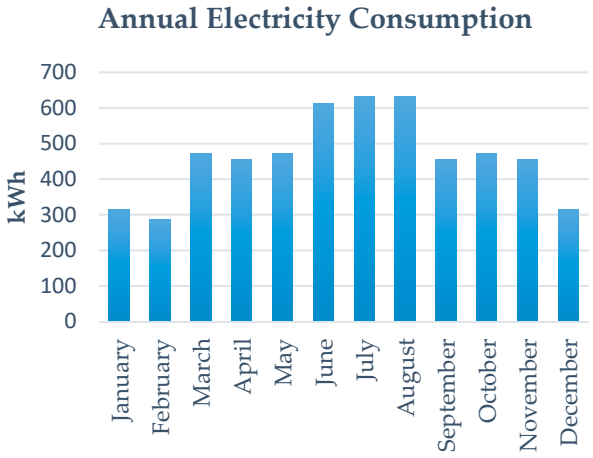

Figure 3. The synthesized electricity consumption of an average four-person household. The estimated baseload of the lowest 3 months was approximately 300 kWh.

A 1 h resolution was used to match the resolution of the PV production profile and to generate 8760 data points of inelastic electricity demand. The electricity profile exhibited seasonal variations and followed the daily human activity in a household peaking twice in a day, i.e., once at midday and once in the evening, similar to [47]. Figure 4 shows the annual load profile in more detail illustrating the hourly peak loads of 2 kWh, 1.4 kWh, and 1.2 kWh generated in the summer, spring/autumn, and winter months, respectively.

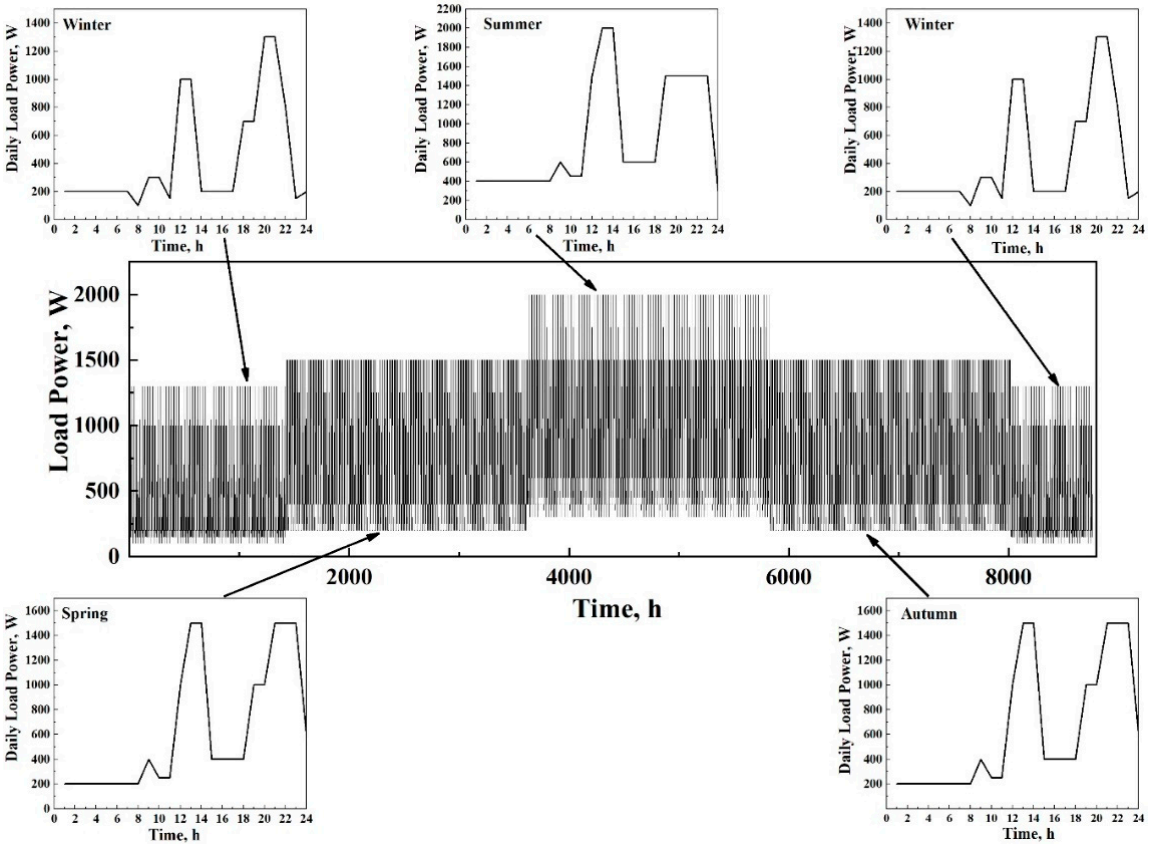

Figure 4. Hourly sequence of the annual load profile, based on the daily electrical appliance usage from a four-person household.

Electricity demand for heating and transportation purposes, flexible loads, and workday/ weekend demand variations were not considered since this would require a more detailed modeling effort; this will be addressed in future work.

2.4. System Operation and Sizing Algorithm

In this section, an operation and sizing algorithm (SA) for autonomous off-grid PVBAT systems is introduced. After the system specification (Step 1 and Step 2 of Figure 1), the SA used time-series data from a TMY of a specified location and consistent data from datasheets of PV, converter, battery, and generator manufacturers to generate annual time series of the power output for one PV module with a 1 h resolution. Initially, numbers for the required PV modules (N) and the required battery nominal energy capacity (Bnec) were set, leading to the determination of the annual PV output power of the entire PV array in hourly steps (P_{pv}) and to the initial battery state of energy (SOE) available. The P_{pv} at this point included converter losses. A matching load profile was synthesized, as described in Section 2.3, leading to an hourly power demand (P_{load}) for an entire year. Figure 5 illustrates the system operation flow in terms of P_{pv} usage, P_{load} coverage, and hourly battery SOE.

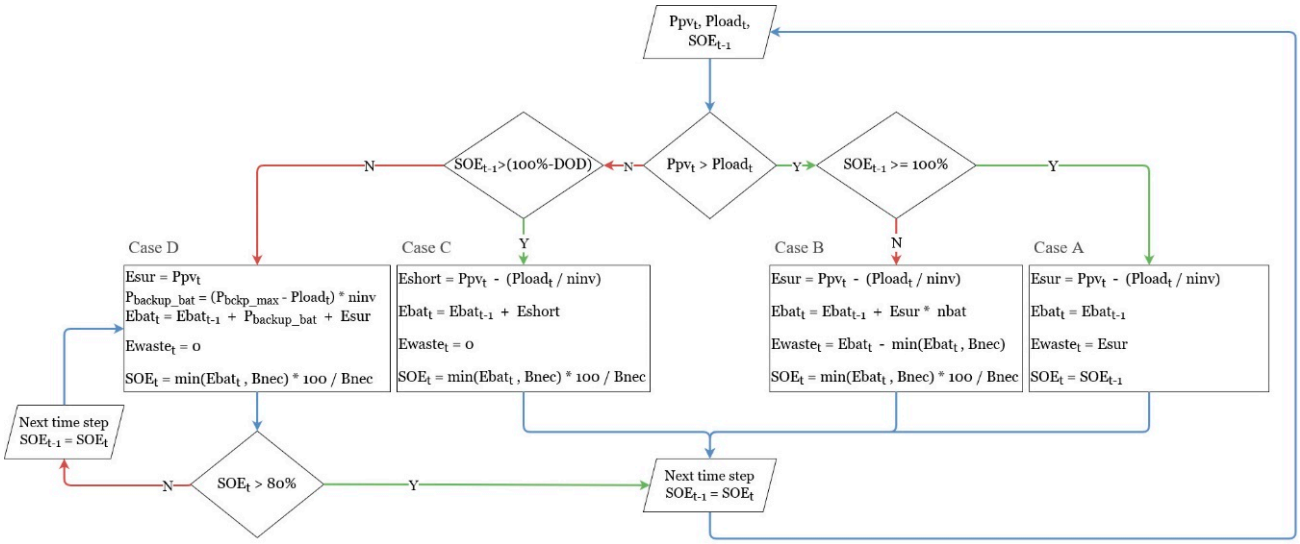

Figure 5. System operation flow according to the to the hourly battery state of energy and PV energy usage.

We can distinguish the following cases of operation depending on whether excess energy is available or not at every hourly step.

Case A. Surplus energy case and a fully charged battery

In this case, available surplus energy, defined here as E_{sur}, should either be used to charge the battery or be discarded.

$$E_{sur} = [P_{PV} - \left(\frac{P_{load}}{n_{inv}}\right)]\Delta t \geq 0, \quad (1)$$

where n_{inv} is the inverter efficiency and can be acquired from the inverter's efficiency curve [26]. The SOE_{t-1} is greater than or equal to 100%, which means that the battery is fully charged, and the excess of PV energy remains unused; thus, potential E_{sur} at this step is wasted and characterized as E_{waste}. With the SOE remaining at the higher level (100%), the algorithm proceeds to the next hourly step with the following equations:

$$E_{waste} = E_{sur}, \quad (2)$$

and

$$SOE_t = SOE_{t-1} \ = \ 100\%. \tag{3}$$

The $t - 1$ indicator means that the calculation of the SOE was made taking into account the data obtained in the previous hourly step.

Case B. Surplus energy case and a partially charged battery

If the $SOE_{t\text{-}1}$ is not greater than or equal to 100%, the battery is in a partially charged state and keeps charging by E_{sur} (Equation (1)). Then, SOE_t which is initially scaled at 100% is defined as follows:

$$SOE_t = \ \frac{\min(Ebat_t, \ B_{nec}) \ \times \ 100}{B_{nec}}. \tag{4}$$

If $Ebat_t < B_{nec}$ with $Ebat_t$ calculated with

$$Ebat_t = Ebat_{t-1} + E_{sur} \times n_{bat}, \tag{5}$$

then the surplus energy (E_{sur}) can be totally absorbed by the battery, where n_{bat} is the charging efficiency of the battery.

If for $Ebat_t$, calculated by Equation (5), $Ebat_t > B_{nec}$ applies, then the amount of energy that cannot be absorbed is discarded.

$$E_{waste} = Ebat_t - \ B_{nec}. \tag{6}$$

Monitoring the above two cases using the algorithm ensures that the SOE is always $\leq$100%. This is the reason why Equation (4) has this form. Afterward, the algorithm proceeds to the next hourly step.

Case C. Energy shortage case

In this case, the PV power output cannot cover the complete inelastic power demand and requires backing to compensate for the energy shortage, defined here as E_{short}.

$$E_{short} = \ [P_{PV} \ - \ \left(\frac{P_{load}}{n_{inv}} \right)]\Delta t < \ 0. \tag{7}$$

The $SOE_{t\text{-}1}$ is greater than the threshold percentage (100%—DOD) which means that the battery is in a partially charged state and keeps discharging as it contributes to the load coverage. Consequently, the SOE_t is defined again by Equation (4), using this time the remaining amount of energy $Ebat_t$, defined by the following equations:

$$Ebat_t = Ebat_{t-1} + E_{short} \ (\mathrm{E_{short}} \ < \ 0), \tag{8}$$

and

$$E_{waste} = 0. \tag{9}$$

Case D. Backup case

If the $SOE_{t\text{-}1}$ is less than the threshold value, which means that the battery is in a discharged state, the backup source needs to start charging the battery in the next hourly step and keep the entire load covered until the battery is fully charged again. This recurring case consists of a loop in which the hourly load is primarily covered by the generator, for loads up to the maximum generator output ($P_{backupMAX}$). Secondarily, the battery is charged with the sum of the power of the remaining generator output on the DC side ($P_{backup\text{->}battery}$) and the available PV power output. Hence, no energy is being discarded (E_{waste} = 0). In this case, the accumulated $Ebat_t$ is described in Equation (13).

$$P_{backup} = \ P_{load} \ + \ \left(P_{backupMAX} \ - \ P_{load} \right), \tag{10}$$

$$P_{backup \rightarrow battery} \ = n_{inv} \times \left(P_{backupMAX} \ - \ P_{load} \right), \tag{11}$$

and

$$E_{sur} = P_{pv}\Delta t, \tag{12}$$

$$Ebat_t = Ebat_{t-1} + P_{backup \to battery} + n_{bat} \times E_{sur}. \tag{13}$$

The SOE_t variation is kept track of by using Equation (4). Breaking out of the loop and returning to normal operation requires that the SOE_t reaches approximately 80%, a safe state that prevents overcharging by an overshooting charge. More specifically, during battery charging by the backup, all the energy generated by the PV system is directed to the battery due to the particular architecture of the system. If we charge the battery further than SOE_t > 80% with the generator, then there is a serious possibility that the contribution of the PV-generated energy gets wasted. Our main concern is always to avoid situations where the energy produced by RES has to be rejected.

On the other hand, energy storage technologies, such as lead–acid batteries, must be fully charged at regular intervals to avoid premature aging, e.g., after a certain number of charge/discharge cycles. This will be integrated into the algorithm in future work.

When the end of the time series is reached, which means that the last hourly step of the simulation has been examined, the results of the simulation are saved. A brief description of the results is shown in Table A1 of Appendix B. Subsequently, a new simulation instance is initiated with incremental *N* and Bnec.

The repetition of this process produces multiple sums of annual discarded energy and annual energy supplied by the generator (ΣE_{waste} + $\Sigma P_{backup}\Delta t$) for every *N* and *Bnec* simulation instance. Therefore, a distinct minimum of ΣE_{waste} + $\Sigma P_{backup}\Delta t$ signifies an optimal *N* and *Bnec* arrangement for which the renewable harvest is maximized. Furthermore, the annually utilized PV output, i.e., the useful energy E_{us}, is defined in Equation (14).

$$E_{us} = \Sigma\left(P_{pv}\Delta t\right) - \Sigma(E_{waste}). \tag{14}$$

Datapoints of the economic unit cost of useful energy are produced in each simulation instance. The distinct minimum of these datapoints signifies an optimal *N* and *Bnec* arrangement for which the cost of every electrical kilowatt-hour generated is essentially minimized.

2.5. System Cost Analysis and the Levelized Cost of Electricity (LCOE)

The performance of different electricity generation technologies can be evaluated by calculating the LCOE [48]. This estimate considers all costs incurred during the lifetime of a power resource with reference to the power resource's total electricity output throughout its complete lifecycle. In this method, the capital cost, as well as the lifecycle cost, which includes operation, maintenance, and replacement expenditures during the power resource's lifetime, are calculated considering an estimated discount factor. Thus, the LCOE is the ratio of the total discounted lifetime cost of a power resource divided by its discounted energy production, and it can be calculated in every simulation instance according to Equation (15).

$$LCOE = \frac{C_{pi} + C_{b,r} + \sum_{n=0}^{24} \frac{C_m + C_{eb} + C_{es}}{(1+i)^n}}{\sum_{n=0}^{24} \frac{E_{us}}{(1+i)^n}} = \frac{C_{pi} + C_{b,r} + (C_m + C_{eb} + C_{es})\left[\frac{(1+i)^n - 1}{i\,(1+i)^n}\right]}{E_{us}\left[\frac{(1+i)^n - 1}{i\,(1+i)^n}\right]}. \tag{15}$$

In this work, the LCOE was calculated in EUR/kWh, where C_{pi} is the total expenditure cost, $C_{b,r}$ is the discounted battery replacement cost, C_m is the annual system maintenance cost, C_{eb} is the annual backup energy cost, C_{es} is the cost of the discarded renewable energy, and E_{us} is the annual useful energy. Similar to the total economic costs at the numerator, the E_{us} at the denominator is also multiplied by a discount factor which is described in

more detail in Appendix A. The annual real interest rate, here i, is estimated using the Fisher equation [49].

$$i = \frac{i' - f}{1 + f}, \tag{16}$$

where i' the nominal interest rate and f the annual inflation rate.

2.5.1. Cost of Battery Replacement ($C_{b,r}$)

The replacement time of batteries (TOR) varies across different accumulator technologies and depends, among other factors, on the number of charge–discharge cycles, as well as on the battery calendar life [50]. Thus, an upper limit calendar life of 5 years was chosen as the maximum TOR for the lead–acid technology, while, for lithium-ion technology, an upper limit calendar life of 10 years was chosen.

Furthermore, in the context of the system's operating cost calculation and to evaluate if the battery needs to be replaced before the abovementioned maximum TOR (TOR_{max}), the number of charge–discharge cycles of the batteries at 100% DOD was estimated according to the total electrical energy delivered by the battery ($Pbat_d$) in a year, using Equation (17).

$$NC = \frac{\sum Pbat_d}{B_{nec}}, \tag{17}$$

where NC is the number of cycles performed by the battery in 1 year. The time of replacement of each battery, expressed in years, was determined using Equation (18).

$$TOR = \frac{Total\ Number\ of\ Cycles\ up\ to\ the\ End\ of\ Life\ at\ 100\%\ DOD}{NC}. \tag{18}$$

The information concerning the numerator of Equation (17) can be retrieved from the battery manufacturer datasheet. In this work, it took the value 500 for lead–acid batteries and the value 2500 for lithium-ion batteries.

When the battery needs to be replaced sooner than the maximum battery calendar life ($TOR < TOR_{max}$), the estimated TOR is taken into account as the replacement time of the battery. In cases where the calculated TOR exceeds the maximum battery calendar life ($TOR > TOR_{max}$), TOR_{max} is considered as the battery replacement time.

Since the guaranteed power output of the PV modules is 25 years, the entire PVBAT system is considered to have the same overall cycle life. Therefore, batteries are conservatively expected to be replaced multiple times over this period. The total cost of battery replacement, at net present value, is calculated using the following equation:

$$C_{b,r} = C_b \sum_{k=0}^{k=n\times TOR<25} \frac{1}{(1+i)^k}, \tag{19}$$

where Cb is the initial battery purchasing cost, k is the year of battery replacement which takes integer values from 0 up to $n \times TOR$, with n receiving the values 1, 2, 3, ... to the point where $n \times TOR < 25$. As mentioned above, the product $n \times TOR$ is only used if $TOR<TOR_{max}$. Otherwise, the product $n \times TOR_{max}$ is used.

2.5.2. Estimations of Annual C_m, C_{eb}, and C_{es}

The annual PVBAT maintenance cost C_m, is the sum of the individual operation and maintenance costs of each system component during a year, including the cost of potential services (e.g., equipment insurance, monitoring services).

The annual backup energy (E_{fuel}), defined in Equation (20), is the required electrical energy to preserve load supply and to charge the batteries via the generator set. This energy is converted from chemical energy contained in diesel fuel and expressed in kWh.

$$E_{fuel} = \frac{\sum P_{bat}}{n_{gen}}, \tag{20}$$

where n_{gen} is the generator efficiency. The annual backup energy cost C_{eb}, defined in Equation (21), is derived from the product of E_{fuel} and the fuel cost ($Fuel_{cost}$) expressed in EUR/lt, divided by the lower heating value (LHV) of diesel fuel, i.e., 9.85 kWh/lt.

$$C_{eb} = \frac{E_{fuel} \times Fuel_{cost}}{LHV}. \quad (21)$$

The cost of the discarded surplus energy C_{es} described in Equation (22) is derived from the product of the annual sum of E_{waste} in kWh and the average LCOE of PV–battery systems expressed in EUR/kWh.

$$C_{es} = \Sigma E_{waste} \times LCOE_{pvbat}. \quad (22)$$

3. Results

3.1. Sizing Simulations

The sizing method proposed in this work is based on the selection of the appropriate number of photovoltaic panels ($N_{optimal}$) and the necessary nominal energy of the energy storage system ($Bnec_{optimal}$), so as to satisfy, without interruptions, the energy consumption profile of an average household for a typical meteorological year in a specified location, whilst minimizing the LCOE expressed by Equation (15).

The initial data required for two distinct and autonomous PV–battery–generator simulation examples are illustrated in Table 1. Both off-grid systems are equal except for aspects concerning the EES technology used. In simulation A, the load supply is facilitated by a lead–acid battery, and, in simulation B, it is facilitated by a lithium-ion battery. In the lead–acid case, the calendar life, cycle life, DOD, and charging efficiency were set to 5 years, 500 cycles, 50%, and 85%, respectively. In the lithium-ion case, the same parameters were set to 10 years, 2500 cycles, 80%, and 98%, respectively. In both cases, the nominal energy content Bnec and the PV module number N were gradually increased in every simulation instance by steps of 5 kWh and two modules, respectively.

Table 1. Input data of two off-grid PV–battery–generator sizing simulations employing different electrical energy storage (EES) technologies. DOD, depth of discharge; SOE, state of energy; BMS, battery management system; LCOE, levelized cost of electricity; LHV, lower heating value.

	Input Parameters	Sim Data A	Sim Data B	Units	Input Type
1	Number of PV modules, N	6 to 34	6 to 34		Physical model assumptions
3	Nominal PV module power, P_{mpp}	310	310	Wp	
2	Nominal energy capacity, Bnec	5 to 30	5 to 30	kWh	
4	Nominal battery cycle life	500	2500	Cycles (100% DOD)	
5	Calendar battery life	5	10	Years	
6	Depth of discharge	50	80	%	
7	$SOE_{t=0}$	100	100	%	
8	Inverter efficiency, n_{inv}	95	95	%	
9	Battery charging efficiency, n_{bat}	85	98	%	
10	P_{backup_max}	4000	4000	W	
11	Number of inverters	1	1		
12	P_{load_max}	4000	4000	W	
13	Battery type	Lead–acid	Lithium-ion		
14	Generator efficiency, n_{gen}	80	80	%	

Table 1. *Cont.*

	Input Parameters	Sim Data A	Sim Data B	Units	Input Type
15	Battery cost	154	574	EUR/kWh	Economic cost assumptions
16	PV module cost	110	110	EUR	
17	Inverter cost	1600	1600	EUR	
18	Monitoring and BMS cost	250	500	EUR	
19	PV mounting system cost	50	50	EUR/mod	
20	Electrical installation cost	1000	1000	EUR	
21	Generator cost	1300	1300	EUR	
22	$LCOE_{pvbat}$	0.26	0.26	EUR/kWh	
23	LHV	9.85	9.85	kWh/lt	
24	Cost of fuel	1.175	1.175	EUR/lt	
25	Real interest rate	0.06919	0.06919	%	
26	Maintenance cost, C_m	160	160	EUR/year	
27	Project years	25	25	Years	

3.2. Performance of Systems

The sizing model described in Section 2.4 of this work was initially validated by examining the change over time of the most important parameters of the PVBAT system for four designated weeks of the year, one for each season. On the basis of the component analysis in Section 2.1.2, the two systems were selected for the presentation of the curves in Figures 6 and 7. Ceteris paribus, one includes lead–acid batteries and the other includes lithium-ion batteries, albeit with different multiples of the nominal energy content. Moreover, both systems exhibit the same PV module type, albeit with different installed capacities.

As the operating model predicts, when the power output from the photovoltaics (black curve) is high and the corresponding SOE (blue curve) is capped at 100%, there is surplus energy that cannot be absorbed (green curve) by the system to charge the batteries or to meet the needs of the load (red curve).

The range in which the SOE varies depends on the battery technology used. In the case of lead–acid technology, a lower limit of 50% was set. We notice that this limit was approached quite often in the first week of the year (winter), while, in the 26th week (summer), the SOE did not receive values less than 60%. On the contrary, since the electricity generation from photovoltaics in winter was lower than in summer months, in winter, the SOE reached its maximum only with energy coming from the backup source, while, in summer, the photovoltaic output alone could fully charge the battery. However, during weeks 13 (spring) and 39 (autumn), the SOE approached its maximum with combined photovoltaic and backup power. Furthermore, on day 5 of week 13 and day 7 of week 39, a significantly reduced PV output at periods with an elevated load causes a temporal undershooting of the lower SOE limit of 50%, thereby briefly draining the battery without triggering the backup source.

A similar behavior is observed in the system where a lithium-ion battery was used, depicted in weeks 1 and 13 of Figure 7. Even though a lower SOE threshold of 20% was set, in the first week (winter), the SOE briefly received values below this threshold. Although this situation does not particularly affect the specific technology, this fact suggests that, to avoid low values for SOE, the control should take place in less than 1 h.

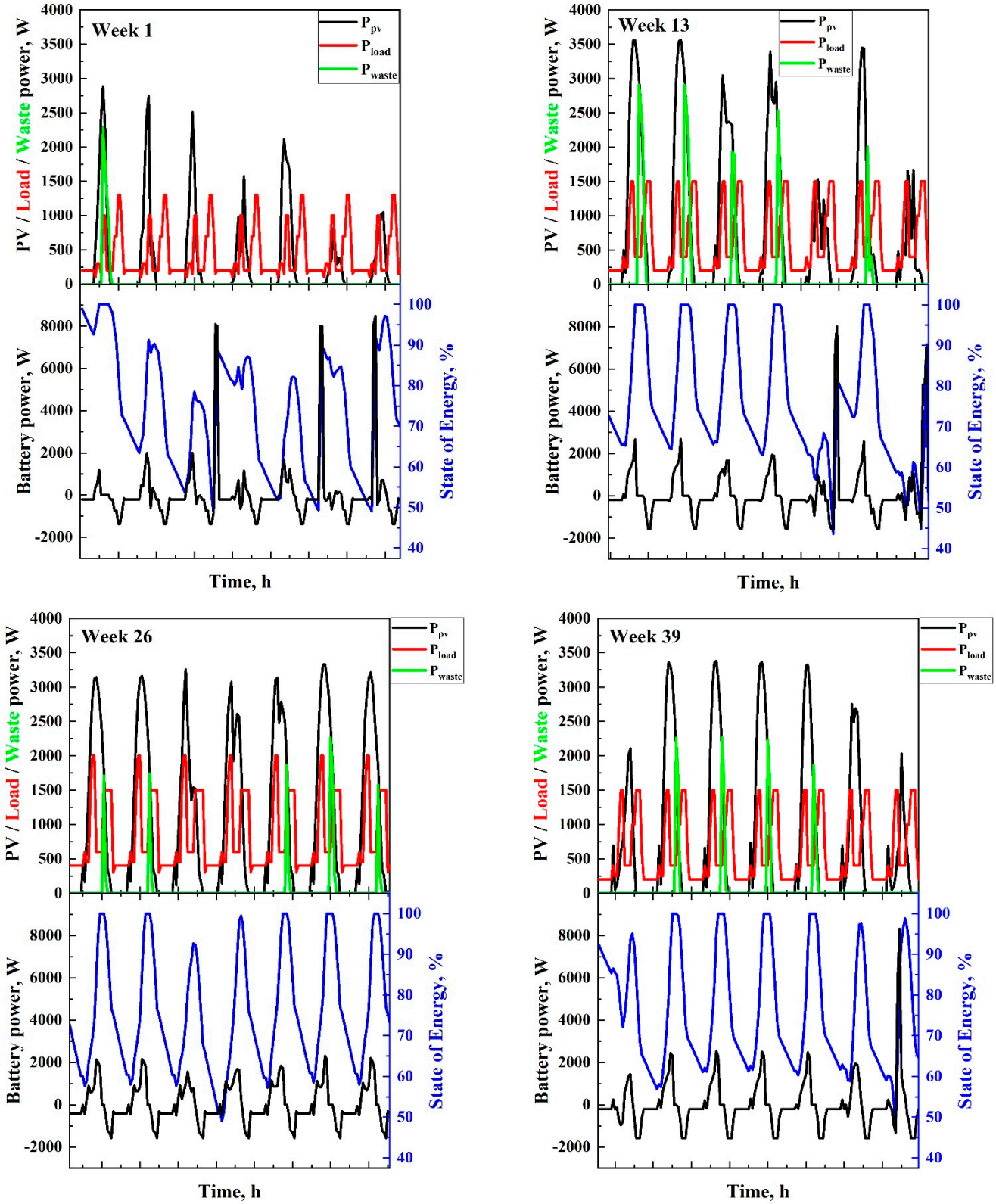

Figure 6. System performance using lead-acid battery.

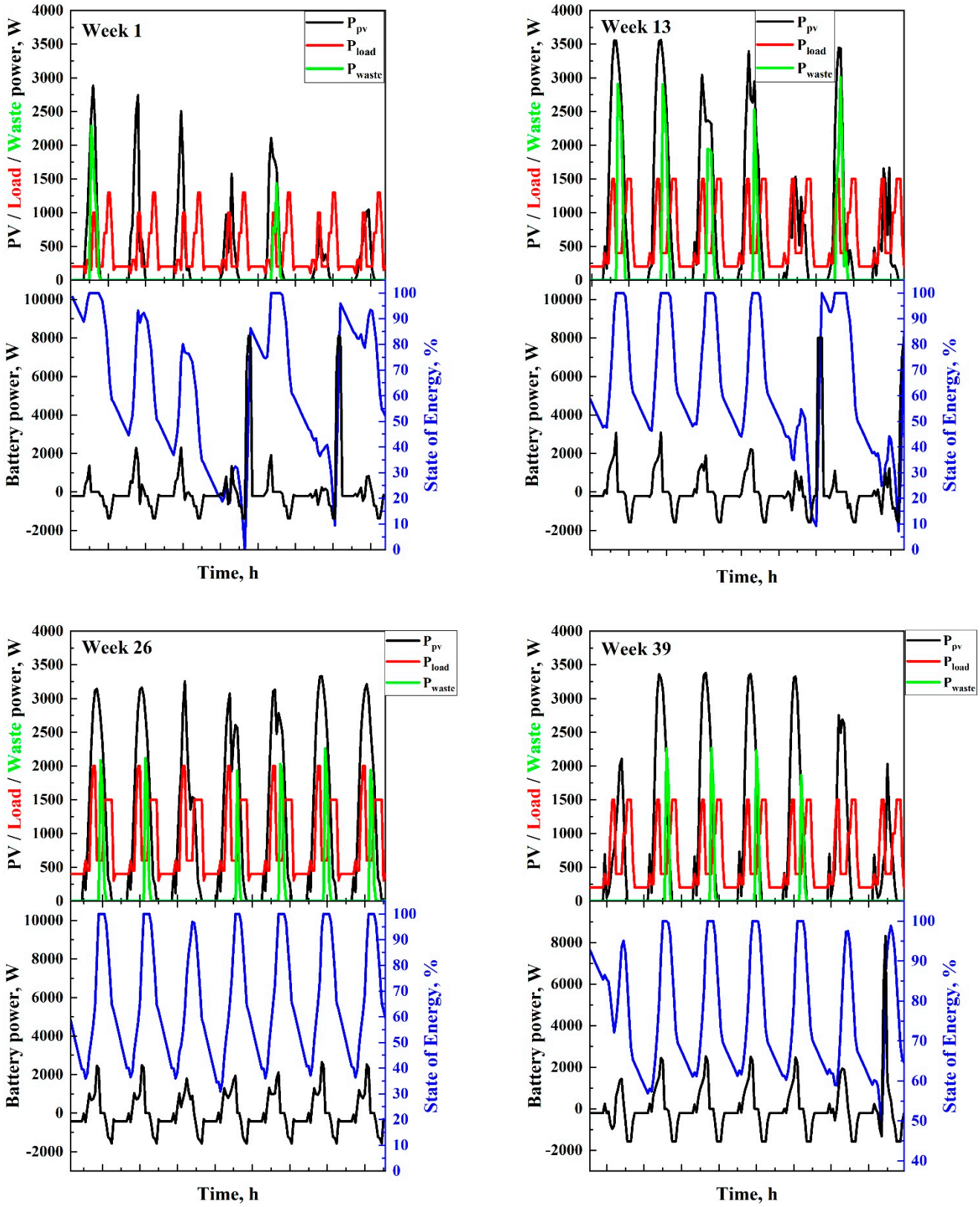

Figure 7. System performance using lithium-ion battery.

3.2.1. Maximizing the Contribution of Solar Energy

The nominal energy content and the module quantity were gradually increased by steps of 5 kWh and 2 modules respectively, forming distinct PV–battery arrangements for every simulation instance of the sizing algorithm.

As the number of photovoltaic panels increases, the solar energy input increases, thus reducing the backup energy required by the generator to cover the load and charge the batteries when the SOE is below the cutoff setting. Moreover, the discarded surplus energy of the system increases, i.e., the solar energy that cannot be absorbed by the system. As evident in Figure 8, maximizing the contribution of renewable energy is achieved when the sum of the backup energy and the discarded surplus energy is minimized.

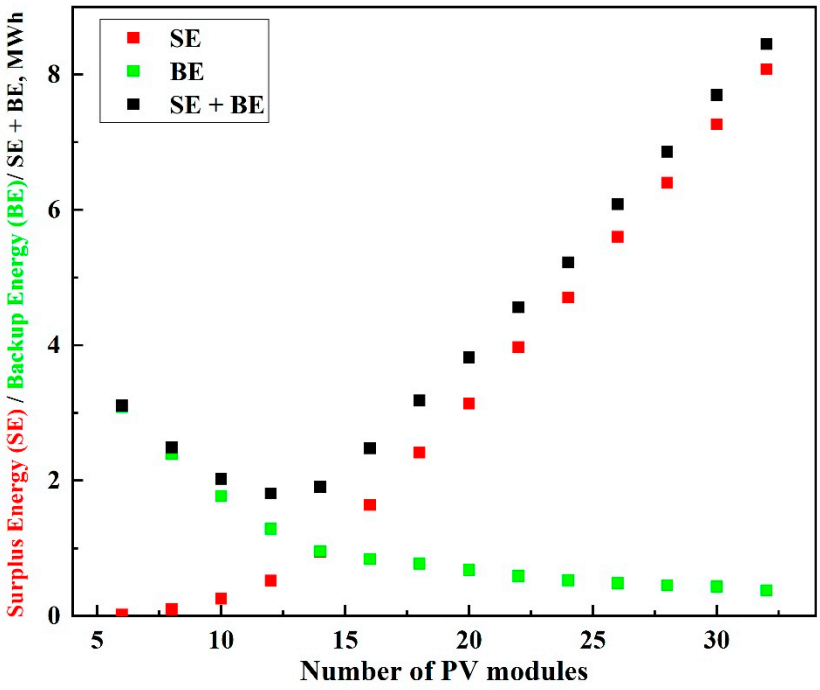

Figure 8. Marker chart depicting 14 simulation instances with constant Bnec and varying PV module number. The descending change of the backup energy and the ascending change of discarded surplus energy indicate the optimal PV panel quantity for which the solar generation is maximized.

This was the case for the simulation instance where the lead–acid battery had a nominal energy content of 30 kWh, where the quantity of PV panels to be used in the system should be 12, as illustrated in Figure 9a. Figure 9b shows the optimal lithium-ion arrangement which happens to be the same as the lead–acid arrangement. The simulations were performed from 6–32 PV panels, the range of which was derived from the ratio of the annual electricity demand to the annual electricity generation, for each N, in every simulation instance, as shown in Equation (23). When considering this ratio, the number of possible simulation instances is reduced significantly, thereby saving computing time in the enumeration process.

$$\frac{\sum_n E_{load}}{\sum_n P_{pv_N}} = \{0.4, \ldots, 2\}. \quad (23)$$

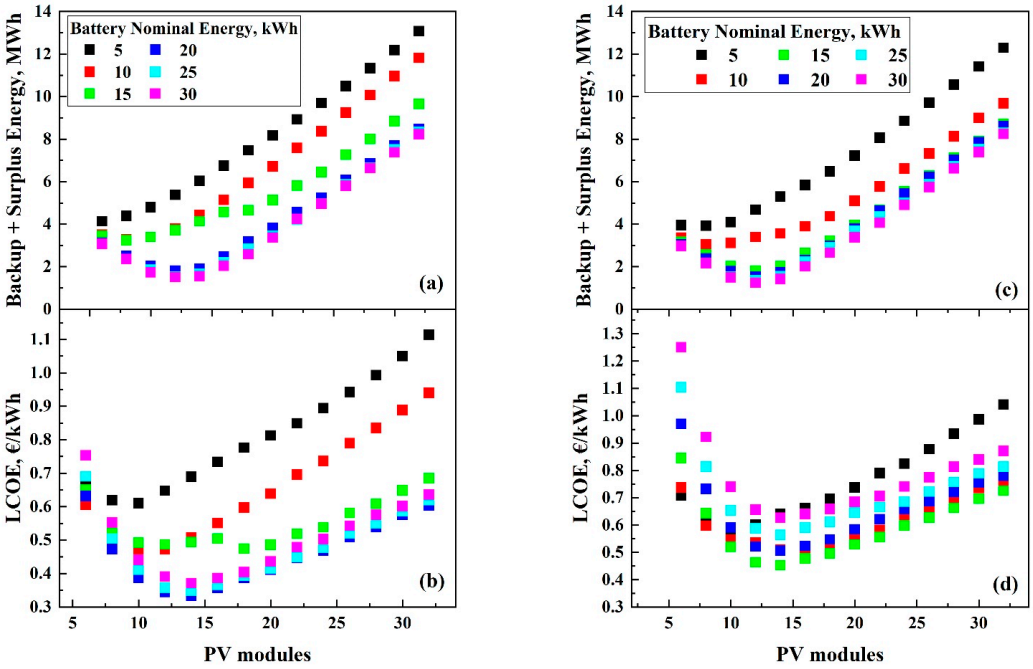

Figure 9. Each marker chart unfolds the optimal *N*–Bnec arrangement in terms of maximal solar energy usage (**a**,**c**) and LCOE minimization (**b**,**d**). Charts 9a and 9b show all the simulation instances of the lead–acid system, while charts 9c and 9d show the results of the lithium-ion system.

The range of Bnec was limited from 5 kWh to 30 kWh, in view of the modular characteristics of the batteries and according to the daily minimum and maximum energy consumption of 1 year.

In both cases, the same behavior was observed: a change in the minimum of each curve to lower values as the nominal battery energy increased. In fact, in the case of lead–acid technology (Figure 9a), the rate of minimum reduction was greatly reduced with the value of 20 kWh of nominal battery energy, while, in the case of lithium-ion technology, this was observed after the nominal energy of 15 kWh. According to the above, the maximization of the solar harvest and, consequently, the minimization of the environmental footprint were achieved using 12 photovoltaic panels and 30 kWh of nominal battery energy in both cases. However, this picture changed when we took into account the financial data of the system for the calculation of the LCOE.

3.2.2. Minimizing the LCOE

The estimation of the LCOE, as defined in Equation (15), was done following the same procedure described previously in Section 2.4. To be more specific, the estimation of the LCOE was performed for two equal PV–battery–generator systems with distinct EES technologies for a nominal battery energy range from 5 kWh to 30 kWh and for 6–32 PV panels. The variation of the LCOE in relation to the quantity of photovoltaic panels is presented in Figure 9b,d for the systems equipped with lead–acid and lithium-ion batteries, respectively.

It is observed that the LCOE curves passed through a minimum. Regarding the system with lead–acid battery, this minimum decreased by increasing the nominal energy of the battery until it reached the value of 20 kWh. After this value, an increase in the LCOE curve's minimum was observed. The same behavior was also noted in the case of lithium-ion batteries with the exception that the nominal energy of the battery, after which the minimum of the LCOE curve began to receive higher values, was 15 kWh. Figure 10 depicts how the minimum value of each curve presented in Figure 9 varied as a function of the nominal energy capacity of the lead–acid and lithium-ion batteries. The same graph includes the optimum number of photovoltaic panels derived by the model.

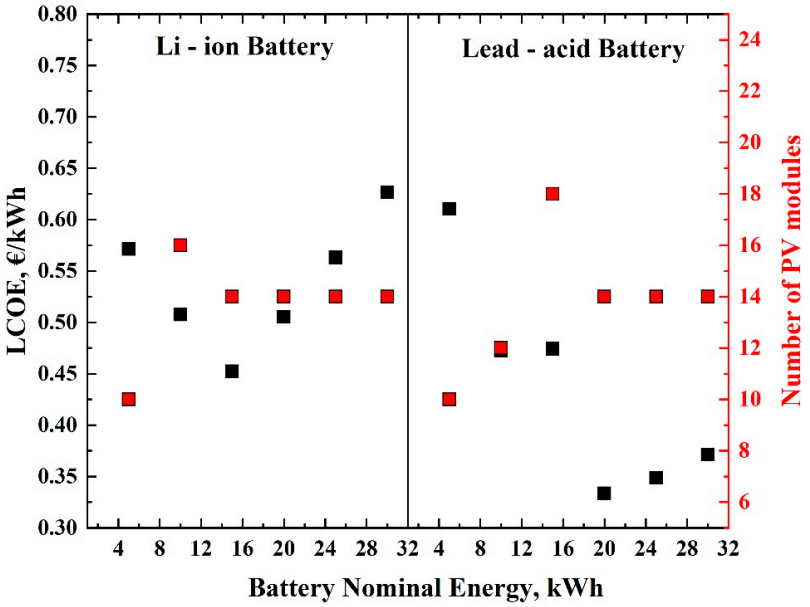

Figure 10. In this marker chart, six simulation instances per EES technology are presented and their calculated LCOEs are directly compared.

One would expect that an increase in the number of PV panels would be accompanied by a corresponding increase in useful energy. This is not the case, since, after a certain point, solar energy cannot be absorbed anymore due to stocked storage resources and limited consumption. This is illustrated in Figure 11 where the annual accumulated useful energy of all simulation instances, in both storage technologies, are shown in contrast to the theoretically optimal photovoltaic electricity generation. Here, after the 14th PV panel, the utilized photovoltaic electricity somewhat stabilized and significantly affected the LCOE of the system, considering that the discounted sum of the generated energy by the system is inversely proportional to the LCOE.

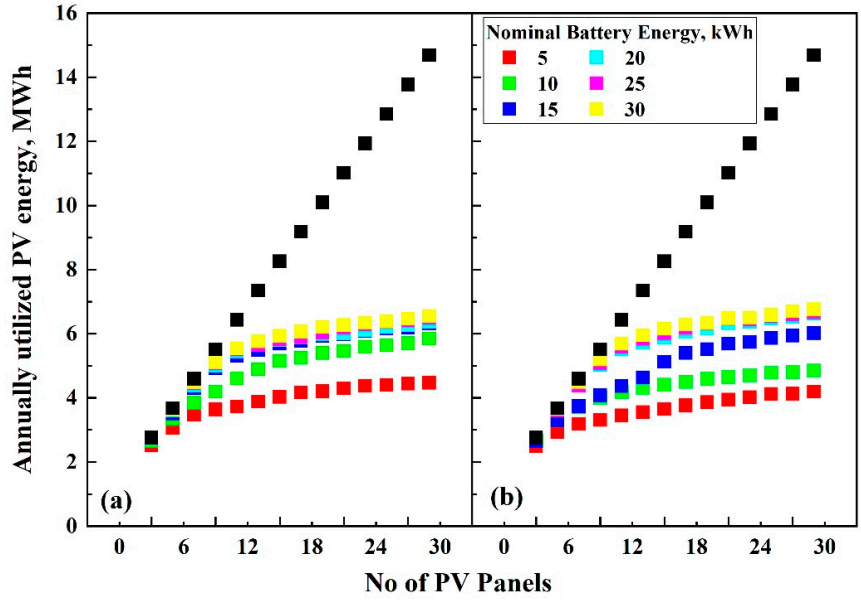

Figure 11. Comparison of the annually utilized PV output E_{us}, as defined in Equation (14), of every lithium-ion (**a**) and lead–acid (**b**) simulation instance and the corresponding theoretically optimal photovoltaic output P_{pv} (black marks).

The calculation of the LCOE, i.e., the unit cost of electricity, requires at first consistent information regarding the capital cost and the operation, maintenance, and replacement expenditures. Subsequently, these financial data can be used to prepare the essential cash flow over a period of 25 years. Table 2 shows the detailed costs for every simulation instance considered in Figure 10. Value added tax was not included, and cost figures refer to the second part of 2020.

Each PV–battery–generator system was considered to have an overall cycle life of 25 years. Standby generator operation was kept below 500 h per year in all instances, with maximal continuous operation limited to 4 h. Premium power electronics were conservatively expected to be replaced every 10 years. The EES calendar life for lithium-ion batteries was set to 10 years, while it was set to 5 years for lead–acid batteries. The determined EES replacement points, ranging from 5–10 years for lithium-ion technology and 1.6–5 years for lead–acid technology, were incorporated in the discounted maintenance cost, listed in the C_{br} column of Table 2.

Table 2. The values of the parameters used to calculate the LCOE at the point where the minimum appeared.

Battery Type	*N* (mods)	Bnec (kWh)	Component Cost				Installation Cost (EUR)	Maintenance Cost		Operation Cost		Eus (kWh/Year)	LCOE (EUR/kWh)
			PV (EUR)	Battery (EUR)	PE&M * (EUR)	Generator (EUR)		C_{br} (Discounted) (EUR)	C_m (EUR/year)	C_{es} (EUR/year)	C_{eb} (EUR/year)		
Lead–Acid	10	5	1100	770	2600	1300	3125	4445	100	369	503	3487.4	0.61
	12	10	1320	1540	2700	1300	3350	4405	100	389	341	4409.8	0.48
	18	15	1980	2310	3000	1300	4025	4289	100	834	215	5557.0	0.47
	14	20	1540	3080	2800	1300	3575	5719	100	247	143	6021.8	0.34
	14	25	1540	3850	2800	1300	3575	7149	100	215	126	6157.9	0.36
	14	30	1540	4620	2800	1300	3575	8579	100	199	117	6226.7	0.38
Lithium-Ion	10	5	1100	2870	2600	1300	3125	4972	100	282	449	3856.2	0.57
	16	10	1760	5740	2900	1300	3800	4446	100	655	205	5306.1	0.51
	14	15	1540	8610	2800	1300	3575	6669	100	301	129	5792.4	0.46
	14	20	1540	11,480	2800	1300	3575	8892	100	265	107	5944.1	0.51
	14	25	1540	14,350	2800	1300	3575	11,115	100	241	92	6047.0	0.57
	14	30	1540	17,220	2800	1300	3575	13,338	100	227	82	6106.0	0.63

* Power Electronics and Monitoring Equipment.

4. Discussion

In this study, a sizing method for autonomous non-interconnected PV–battery systems backed by a standby power source was presented. Emphasis was placed on monocrystalline photovoltaics in conjunction with DC-coupled EES systems supplying electricity to a typical inelastic load profile. The standby power was simulated in the form of a diesel generator set, taking into account the CTU, APT, and ALV thresholds. The operation and sizing algorithm described in Section 2.4 was studied and validated by examining the variation of important system parameters for four designated weeks of the year, one for each season. The algorithm calculated, among other factors, the useful energy Eus, a key output parameter for which the solar harvest is maximized in parallel with the minimization of the LCOE.

The results showed that the LCOE varied in different configurations with respect to system component selection and design principles. The results also indicated a fairly downward trend of the LCOE of PV–battery systems. More specifically, the LCOE was calculated using Eus in the denominator of Equation (15). Furthermore, for every increase in the nominal battery energy capacity Bnec in every simulation instance, an increase in useful energy output was observed (Figure 11). Hence, if one disregarded the LCOE, the sizing method would eventually point to a configuration which, on the one hand, would fully exploit the available solar energy but, on the other hand, would lead to an oversized battery. This is a weak point in most sizing algorithms since an oversized battery entails a higher carbon footprint and increased costs. However, in this study, the lowest LCOE was found to be 0.34 EUR/kWh for systems using lead–acid batteries, whereas, for systems using lithium-ion batteries, the LCOE was found to be 0.46 EUR/kWh, which are both considerably lower estimations than those which appeared in several other studies [25,51].

Another critical aspect to consider is the backup energy source to be used. In this study, a standby diesel generator set was selected as a backup to compensate for energy shortages due to intermittencies from renewables. Low battery SOE in the absence of solar irradiance initiates the generator set, which in turn commences the charging loop until the SOE is equal to or greater than 80%. The upper charging limit was set to 80% to ensure that the PV and the generator would not overcharge the battery and discard energy. This of course means that, especially in winter when the generator needs to be used more often, the battery may have to operate at a partial state of charge. However, this is not a deterrent, as pointed out in [52,53]. The total generator output supplies power to the prioritized load on the AC bus, and the remaining power is used to charge the battery on the DC bus. Thus, CTU is equal to the battery charging time. Since the nominal power output of the generator set was fixed, battery charging time increased in line with the increase in Bnec, which can be confirmed from the CTU column in Table 3. Simulation instances where CTU exceeded 5 h were ignored. The ALV was kept constant, disregarding battery charging profiles for simplification. Therefore, the generator was expected to operate invariably at high-efficiency levels constantly providing the maximum power output, as is seen in the ALV column of Table 3. In instances of lithium-ion batteries, elevated charging times were mainly attributable to the greater DOD of this accumulator technology. On the contrary, lead–acid batteries require more annual generator operation time than lithium-ion batteries, with APT ranging from 873 h to 196 h.

Table 3. The maximum continuous time use (CTU), the estimated annual operation time (APT), and the average load value (ALV) of the standby diesel genrator in diverse simulation arrangemnets.

Battery Type	*N* (mods)	Bnec (kWh)	CTU (h)	APT (h/year)	ALV (kW)
Lead–Acid	10	5	1	873	4000
	12	10	2	571	4000
	18	15	2	360	4000
	14	20	3	239	4000
	14	25	3	211	4000
	14	30	4	196	4000
Lithium-Ion	10	5	1	784	4000
	16	10	3	343	4000
	14	15	4	216	4000
	14	20	5	180	4000
	14	25	5	158	4000
	14	30	6	137	4000

Furthermore, battery aging calculated in this work provides a more realistic way to find battery replacement time than in the literature [7,9,13]. This is due to the fact that it takes into account the total energy amount removed from the battery compared to the manufacturer's specifications. However, a weak point of the method is the use of SOE instead of state of charge (SOC). More specifically, the use of SOE does not take into account the rate at which the battery is charged and discharged as is the case with SOC [16,54]. This means that, at high rates of battery charging and discharging, the SOE method allows us to transfer power to and from the battery without any restriction except for the maximum and minimum limit whereas, in the case of the SOC, under the same conditions, the energy amounts may be smaller. Although the appearance of high currents in applications using renewable energy sources in non-interconnected systems is not frequent, future study of this method using SOC is one of the objectives of our research team.

5. Conclusions

One reason for an increase in global energy demand is economic growth, which is strongly related to higher energy use. Power systems that take advantage of renewable energy sources, in conjunction with energy storage systems, are effectively addressing the challenge of rural and remote electrification while mitigating greenhouse gas emissions.

This study proposes a sizing method for off-grid electrification systems consisting of photovoltaics, batteries, and a diesel generator set, which are based on the selection of the appropriate quantity of PV panels and battery energy capacity whilst minimizing the LCOE. An operation and sizing algorithm was presented, which used TMY time series of a specified location and consistent data from datasheets of PV, converter, battery, and generator manufacturers, to generate annual time series of the power output for one PV module, eventually determining the annual PV output of an entire PV array in hourly steps. The algorithm calculates, among other factors, the useful energy Eus, a key output parameter for which the solar harvest is maximized in parallel with the minimization of the LCOE. A load profile was synthesized and matched against the computed PV power output. Optimal operation is validated by examining the change over time of the most important parameters for different PVBAT systems utilizing lead–acid and lithium-ion batteries.

Sizing was done for two single-phase DC-coupled PVBG systems differing only in the applied battery technology, i.e., lead–acid and lithium-ion. Both systems used one inverter (5000 VA) and one diesel generator (6000 VA). Test results showed that, for a given annual load of approximately 5570 kWh, the optimal PV array size for both systems consisted of 14 modules (310 Wp/mod). The optimal nominal energy capacity for the lead–acid

system was 20 kWh and that for the lithium-ion system was 15 kWh. The lead–acid system utilized 6021.8 kWh of electrical energy and wasted approximately 922.2 kWh renewable energy, whereas the lithium-ion system utilized 5792.4 kWh and wasted approximately 1117.9 kWh. The solar harvest was maximized in both cases in a different configuration, i.e., using 12 photovoltaic panels and 30 kWh of battery nominal energy capacity. The estimated LCOE for systems using lead–acid batteries was 0.34 EUR/kWh, while it was 0.46 EUR/kWh for systems using lithium-ion batteries. Further consideration of technical aspects of the auxiliary generator set and EES technologies led to the determination of capital costs, replacement costs, operation and maintenance costs, and fuel costs. The tests also revealed a weak point. The sizing algorithm applied in this study constitutes an enumerative rule-based method and is, therefore, central processing unit (CPU)-intensive. This means that the total number of simulation instances (N and Bnec combinations) is a tradeoff between accuracy and runtime speed. Nevertheless, runtime remains relatively brief for small-scale applications. In large-scale applications, this can be overcome by intuitively limiting the N and Bnec values.

Applying the methodology used in the present study, a proposal for future work involves mapping the LCOE, using geographic information systems, while addressing the meteorological uncertainties of various isolated areas such as islands. Especially in areas without a power grid, comparing different backup energy systems and their uncertainties could give some additional insights into varying electricity generation costs. Another recommendation for future work includes the development of a method for generating distributions of load profiles according to consumption category, which would lead to a more general application of the methodology proposed in this work.

Author Contributions: Conceptualization, methodology, software, validation, and writing—review and editing, C.E. and I.E.K. Both authors have read and agreed to the published version of the manuscript.

Funding: This research received no external funding.

Conflicts of Interest: The authors declare no conflict of interest.

Nomenclature

ALV	Average load value of diesel generator
AOI	Angle of incidence
APT	Annual operation time of diesel generator
BMS	Battery management system
Bnec	The required battery energy capacity
Cb,r	Discounted battery replacement cost,
Ceb	Annual backup energy cost
Ces	Cost of the discarded renewable energy
Cm	Annual system maintenance cost
Cpi	Total capital cost
CTU	Maximum continuous time use of diesel generator
DER	Distributed energy resource
DHI	Diffuse horizontal irradiance
DNI	Direct normal irradiance
DOD	Depth of discharge
Ebatt	The remaining amount of energy that is transferred to the battery at time t
EES	Electrical energy storage
Eshort	Energy shortage when the PV output cannot cover the power demand
Esur	Surplus energy
Eus	Annually utilized PV energy output

Ewaste	Excess solar power that remains unused
GHI	Global horizontal irradiance
I0	Diode reverse saturation current
IL	Photocurrent
LCOE	Levelized cost of electricity
LPG	Liquefied petroleum gas
MPPT	Maximum power point tracking
N	The required PV module number
nbat	Charging efficiency of the battery
ninv	Inverter efficiency
nNsVth	Modified diode ideality factor
$P_{backup->battery}$	The remaining generator output on the DC side charging the battery
$P_{backupMAX}$	Maximum diesel generator output
PERC	Passivated emitter and rear contact PV module
Pload	The hourly power demand for in a year.
Ppv	Hourly PV power output in a year
PVBG	Photovoltaic system with batteries and generator set
PVLIB	Solar simulation library for PV energy systems
Rs	Series resistance
Rsh	Shunt resistance
SA	Operation and sizing algorithm
SOE	Battery state of energy
SOE	Battery state of energy (SOE) available
STC	Standard test conditions
T	Atmospheric temperature
TC	PV cell temperature
TM	PV module temperature
TMY	Typical meteorological year
WS	Horizontal windspeed

Appendix A

Proof of relationship:

$$\sum_{1}^{n} \frac{1}{(1+i)^n} = \frac{(1+i)^n - 1}{(1+i)^n i}. \tag{A1}$$

The left-hand side of the (A1) becomes

$$\sum_{1}^{n} \frac{1}{(1+i)^n} = \frac{1}{(1+i)^1} + \frac{1}{(1+i)^2} + \ldots . + \frac{1}{(1+i)^n}.$$

Setting $(1+\mathrm{i}) = \mathrm{x}$ yields

$$\sum_{1}^{n} \frac{1}{x^n} = \frac{1}{x^1} + \frac{1}{x^2} + \ldots . + \frac{1}{x^n}.$$

Multiplying with $\frac{(x-1)}{(x-1)}$ yields

$$\frac{(x-1)}{(x-1)}\left(\frac{1}{x^1} + \frac{1}{x^2} + \ldots . + \frac{1}{x^n}\right) = \frac{1}{(x-1)}\left(1 + \frac{1}{x^1} + \ldots . + \frac{1}{x^{n-1}} - \frac{1}{x^1} - \frac{1}{x^2} - \ldots . - \frac{1}{x^n}\right) =$$
$$\frac{1}{(x-1)}\left(1 - \frac{1}{x^n}\right) = \frac{x^n - 1}{x^n(x-1)} = \frac{(1+i)^n - 1}{(1+i)^n(1+i-1)} = \frac{(1+i)^n - 1}{(1+i)^n i}.$$

Appendix B

Table A1. Description of simulation parameters acquired on every simulation instance.

	Parameter	Description
p.1	Bnec	The minimum multiple battery nominal energy capacity, in Wh.
p.2	N	The PV module number in an array.
p.3	Σ(Ppv)	The sum of hourly PV power output in a year, in Wh.
p.4	Σ(Pload)	The sum of the hourly power demand on the consumption side in a year, in Wh.
p.5	Σ(Pbat,d)	The annual sum of energy discharging the battery, in Wh.
p.6	Σ(Pbat,ch)	The annual sum of energy charging the battery, in Wh.
p.7	Σ(Ewaste)	The annual sum of unused (discarded) energy, in Wh.
p.8	Σ(Pbackup)	The annual sum of the generator output, in Wh.
p.9	Σ(Pbackup->bat)	The annual sum of energy flowing from the generator to the battery, in Wh.
p.10	Σ(Backup_Operation)	The sum of operational hours of the generator in a year.
p.11	Σ(Pload)_Σ(Ppv)_ratio	The ratio of the annual PV power output to the annual power demand.
p.12	Battery_Cycles	Battery_Cycles = abs(Σ(Pbat,d))/Bnec The total charge–discharge cycles of the battery for a year.
p.13	Σ(Ewaste) + Σ(Pbackup)	The sum of annual discarded energy and annual energy supplied by the generator, in Wh.
p.14	Eus	= Σ(Ppv) − Σ(Ewaste) Useful_Energy The utilized PV output, in Wh.
p.15	Bat_Replac_Years	= NBC/Battery_Cycles Where NBC is the nominal battery cycle life stated by the battery manufacturer in the datasheet.
p.16	PV_Cost(N)	= $N \times$ PV_Module_Cost The capital cost of PV panels.
p.17	Battery_Cost_Lead	= (Bnec/1000) × Bat_Cost_Lead–Acid, where Bat_Cost_Lead–Acid is the battery capital cost per kWh.
p.18	Battery_Cost_Lithium	= (Bnec/1000) × Bat_Cost_LiFePO4, where Bat_Cost_LiFePO$_4$ is the battery capital cost per kWh.
p.19	Power_Electr_Cost(N)	= Inverter_Cost + Monitoring_Cost + $N \times 50$, in EUR. The capital cost for power electronics depends on the number of PV panels installed. The above function is an approximation and can usually be derived by the power electronics distributor pricelist.
p.20	Mounting_Cost(N)	= $N \times$ 1_Panel_Roof_Mounting_Cost. The capital cost for PV mounting systems can vary significantly depending on site-specific individualities. Although, in this work, a simple dependency on the amount of PV panels was acceptable, a more precise cost estimation must be considered in demanding installation sites.
p.21	Installation_Service_Cost(N)	= Electrical_Install_Cost + Mounting_Cost(N), where Electrical_Install_Cost is the service cost for the indoor electrical construction, i.e., the power electronics–battery–wiring setup. Installation_Service_Cost(N) is also dependent on the amount of installed PV panels since more modules generally mean more converters, batteries, cabling, and mounting stands to install. This is an empirically determined quantity and scaled to the size of the total PV installation.

Table A1. *Cont.*

	Parameter	Description
p.22	Electr&Install_Materials(N)	= $N \times 12.5$ + Electrical_Install_Cost, in Euro. The material purchasing and installation cost for the electrical wiring, and construction, consisting mainly of low voltage protection and control equipment (Miniature circuit breakers (MCBs), wires, enclosure, switchboards, etc.). This is also an empirically determined quantity, scaled to the number of PV panels and dependent on the service cost for the indoor electrical construction.
p.23	Σ_COST_(PV&Lead-Acid)	= [PV_Cost(N) + Battery_Cost_Lead + Power_Electr_Cost(N) + Mounting_Cost(N) + Installation_Service_Cost + Electr&Install_Materials]
p.24	Σ_COST_(PV&LiFePO4)	= [PV_Cost(N) + Battery_Cost_Lithium + Power_Electr_Cost(N) + Mounting_Cost(N) + Installation_Service_Cost + Electr&Install_Materials]
p.25	Σ_Bat_Repl_Cost_Lead	Accumulation of net present value battery replacement cost for lead–acid batteries.
p.26	Σ_Bat_Repl_Cost_Lithium	Accumulation of net present value battery replacement cost for $LiFePO_4$ batteries.
p.27	Efuel	= Σ(Pbackup)/ngen The fuel energy required by the generator to cover the load and battery demand, in kWh per year.
p.28	Ces	= Σ(Ewaste) × $LCOE_{PVBAT}$/1000 The unit cost of the discarded energy, based on the estimated LCOE of a typical PV-Battery setup, approximately 0.26 EUR/kWh.
p.29	Ceb	= Efuel × Cost_of_Fuel/Fuel_energy_vol Cost_of_Fuel = 1.175 EUR/L and Fuel_energy_vol = 9850
p.30	Cost_of_Energy	= [(Ces + Ceb) × ((1 + Real_Interest) ^ (Project_Years + 1) − 1)/(Real_Interest × (1 + Real_Interest) ^ Project_Years)]
p.31	Total_Cost	= T + Generator_Cost + Σ_Bat_Repl_Cost + Cost_of_Energy, where T = [Σ_COST_(PV&Lead–Acid) or Σ_COST_(PV&$LiFePO_4$)]
p.32	TC_UE_ratio	= Total_Cost/ΣUseful_Energy (EUR/kWh)

References

1. REN21. *Renewables 2020 Global Status Report*; REN21 Secretariat: Paris, France, 2020; ISBN 978-3-948393-00-7.
2. El-houari, H.; Allouhi, A.; Rehman, S.; Buker, M.S.; Kousksou, T.; Jamil, A.; El Amrani, B. Design, Simulation, and Economic Optimization of an Off-Grid Photovoltaic System for Rural Electrification. *Energies* **2019**, *12*, 4735. [CrossRef]
3. Bahramara, S.; Parsa Moghaddam, M.; Haghifam, M.R. Optimal planning of hybrid renewable energy systems using HOMER: A review. *Renew. Sustain. Energy Rev.* **2016**, *62*, 609–620. [CrossRef]
4. Khatib, T.; Ibrahim, I.A.; Mohamed, A. A review on sizing methodologies of photovoltaic array and storage battery in a standalone photovoltaic system. *Energy Convers. Manag.* **2016**, *120*, 430–448. [CrossRef]
5. Hina Fathima, A.; Palanisamy, K. Optimization in microgrids with hybrid energy systems—A review. *Renew. Sustain. Energy Rev.* **2015**, *45*, 431–446. [CrossRef]
6. Dufo-López, R.; Bernal-Agustín, J.L.; Yusta-Loyo, J.M.; Domínguez-Navarro, J.A.; Ramírez-Rosado, I.J.; Lujano, J.; Aso, I. Multi-objective optimization minimizing cost and life cycle emissions of stand-alone PV-wind-diesel systems with batteries storage. *Appl. Energy* **2011**, *88*, 4033–4041. [CrossRef]
7. Maleki, A.; Askarzadeh, A. Optimal sizing of a PV/wind/diesel system with battery storage for electrification to an off-grid remote region: A case study of Rafsanjan, Iran. *Sustain. Energy Technol. Assess.* **2014**, *7*, 147–153. [CrossRef]
8. Wei, Z.; Li, X.; Xu, L.; Cheng, Y. Comparative study of computational intelligence approaches for NOx reduction of coal-fired boiler. *Energy* **2013**, *55*, 683–692. [CrossRef]
9. Ghafoor, A.; Munir, A. Design and economics analysis of an off-grid PV system for household electrification. *Renew. Sustain. Energy Rev.* **2015**, *42*, 496–502. [CrossRef]
10. Mandelli, S.; Brivio, C.; Colombo, E.; Merlo, M. A sizing methodology based on Levelized Cost of Supplied and Lost Energy for off-grid rural electrification systems. *Renew. Energy* **2016**, *89*, 475–488. [CrossRef]
11. Mandelli, S.; Brivio, C.; Colombo, E.; Merlo, M. Effect of load profile uncertainty on the optimum sizing of off-grid PV systems for rural electrification. *Sustain. Energy Technol. Assess.* **2016**, *18*, 34–47. [CrossRef]

12. Shang, C.; Srinivasan, D.; Reindl, T. An improved particle swarm optimization algorithm applied to battery sizing for stand-alone hybrid power systems. *Int. J. Electr. Power Energy Syst.* **2016**, *74*, 104–117. [CrossRef]
13. Rodríguez-Gallegos, C.D.; Yang, D.; Gandhi, O.; Bieri, M.; Reindl, T.; Panda, S.K. A multi-objective and robust optimization approach for sizing and placement of PV and batteries in off-grid systems fully operated by diesel generators: An Indonesian case study. *Energy* **2018**, *160*, 410–429. [CrossRef]
14. Li, J. Optimal sizing of grid-connected photovoltaic battery systems for residential houses in Australia. *Renew. Energy* **2018**, *136*, 1245–1254. [CrossRef]
15. Wu, J.; Wei, Z.; Liu, K.; Quan, Z.; Li, Y. Battery-Involved Energy Management for Hybrid Electric Bus Based on Expert-Assistance Deep Deterministic Policy Gradient Algorithm. *IEEE Trans. Veh. Technol.* **2020**, *69*, 12786–12796. [CrossRef]
16. Wu, J.; Wei, Z.; Li, W.; Wang, Y.; Li, Y.; Sauer, D.U. Battery Thermal- and Health-Constrained Energy Management for Hybrid Electric Bus Based on Soft Actor-Critic DRL Algorithm. *IEEE Trans. Ind. Inform.* **2021**, *17*, 3751–3761. [CrossRef]
17. Aldersey-Williamsa, J.; Rubert, T. Levelized cost of energy—A theoretical justification and critical assessment. *Energy Policy* **2019**, *124*, 169–179. [CrossRef]
18. Lai, C.S.; McCulloch, M.D. Levelized cost of electricity for solar photovoltaic and electrical energy. *Appl. Energy* **2017**, *190*, 191–203. [CrossRef]
19. Available online: https://www.energy.gov/eere/solar/crystalline-silicon-photovoltaics-research (accessed on 20 January 2021).
20. Available online: https://www.nrel.gov/docs/fy20osti/77010.pdf (accessed on 20 January 2021).
21. Available online: https://www.solarcall.it/home-en/download (accessed on 20 January 2021).
22. Kosmadakis, I.; Elmasides, C. Towards performance enhancement of hybrid power supply systems based on renewable energy sources. *Energy Procedia Elsevier* **2018**, *157*, 977–991. [CrossRef]
23. Available online: https://www.victronenergy.gr/media/pricelist/WEB_WithoutIP65_PricelistVictron2020-Q4.pdf (accessed on 20 January 2021).
24. Ayeng'o, S.P.; Schirmer, T.; Kairies, K.; Axelsen, H.; Sauer, D.U. Comparison of off-grid power supply systems using lead-acid and lithium-ion batteries. *Sol. Energy* **2018**, *162*, 140–152. [CrossRef]
25. Kosmadakis, I.E.; Elmasides, C.; Eleftheriou, D.; Tsagarakis, K.P. A Techno-Economic Analysis of a PV-Battery System in Greece. *Energies* **2019**, *12*, 1357. [CrossRef]
26. Liu, N.; Senthil, R.A.; Zhang, X.; Pan, J.; Sun, Y.; Liu, X. A green and cost-effective process for recovery of high purity α-PbO from spent lead acid batteries. *J. Clean. Prod.* **2020**, *267*, 122107. [CrossRef]
27. Available online: https://www.systems-sunlight.com/wp-content/uploads/2018/10/sunlight_res_sopzv_eu_us_2_19_6p_web_final.pdf (accessed on 20 January 2021).
28. Available online: https://www.victronenergy.com/upload/documents/Datasheet-12,8-&-25,6-Volt-lithium-iron-phosphate-batteries-Smart-EN.pdf (accessed on 20 January 2021).
29. Keil, P.; Schuster, S.F.; Wilhelm, J.; Travi, J.; Hauser, A.; Karl, R.C.; Jossen, A. Calendar Aging of Lithium-Ion Batteries. *J. Electrochem. Soc.* **2016**, *163*, A1872. [CrossRef]
30. Li, D.; Danilov, D.L.; Xie, J.; Raijmakers, L.; Gao, L.; Yang, Y.; Notten, P.H.L. Degradation Mechanisms of C6/LiFePO4 Batteries: Experimental Analyses of Calendar Aging. *Electrochim. Acta* **2016**, *190*, 1124–1133. [CrossRef]
31. Yilmaz, S.; Dincer, F. Optimal design of hybrid PV-Diesel-Battery systems for isolated lands: A case study for Kilis, Turkey. *Renew. Sustain. Energy Rev.* **2017**, *77*, 344–352. [CrossRef]
32. Marqusee, J.; Jenket, D. Reliability of emergency and standby diesel generators: Impact on energy resiliency solutions. *Appl. Energy* **2020**, *268*, 114918. [CrossRef]
33. Benton, K.; Yang, X.; Wang, Z. Life cycle energy assessment of a standby diesel generator set. *J. Clean. Prod.* **2017**, *149*, 265–274. [CrossRef]
34. Kosmadakis, I.E.; Elmasides, C.; Koulinas, G.; Tsagarakis, K.P. Energy Unit Cost Assessment of Six Photovoltaic-Battery Configurations. *Renew. Energy* **2021**. [CrossRef]
35. Maxwell, E.L. A Quasi-Physical Model for Converting Hourly Global to Direct Normal Insolation. August 1987; (SERI/TR-215-3087); pp. 35–46. Available online: http://rredc.nrel.gov/solar/pubs/PDFs/TR-215-3087.pdf (accessed on 21 August 2018).
36. Loutzenhiser, P.G.; Manz, H.; Felsmann, C.; Strachan, P.A.; Frank, T.; Maxwell, G.M. Empirical validation of models to compute solar irradiance on inclined surfaces for building energy simulation. *Sol. Energy* **2007**, *81*, 254–267. [CrossRef]
37. King, D.L.; Boyson, W.E.; Kratochvil, J.A. Photovoltaic Array Performance Model. Sandia Report 2004 (SAND2004-3535). Available online: http://www.osti.gov/servlets/purl/919131-sca5ep/ (accessed on 17 August 2018).
38. De Soto, W.; Klein, S.A.; Beckman, W.A. Improvement and Validation of a Model for Photovoltaic Array Performance. *Sol. Energy* **2006**, *80*, 78–88. [CrossRef]
39. Hongmei, T.; Mancilla-David, F.; Ellis, K.; Muljadi, E.; Jenkins, P. A Cell-to-Module-to-Array Detailed Model for Photovoltaic Panels. *Sol. Energy* **2012**, *86*, 2695–2706.
40. Gray, J.L. *The Physics of the Solar Cell*; John Wiley & Sons, Ltd.: Hoboken, NJ, USA, 2003; Chapter 3; pp. 62–112. ISBN 0-471-49196-9. [CrossRef]
41. Holmgren, W.F.; Hansen, C.W.; Mikofski, M.A. pvlib python: A python package for modeling solar energy systems. *J. Open Source Softw.* **2018**, *3*, 884. [CrossRef]

42. Stein, J.S.; Holmgren, W.F.; Forbess, J.; Hansen, C.W.H. PVLIB: Open Source Photovoltaic Performance Modeling Functions for Matlab and Python. In Proceedings of the IEEE 44th Photovoltaic Specialist Conference, Portland, OR, USA, 5–10 June 2017; pp. 3425–3430.
43. Andrews, R.W.; Stein, J.S.; Hansen, C.W.H.; Riley, D. Introduction to the Open Source PV LIB for Python Photovoltaic System Modelling Package. In Proceedings of the IEEE 40th Photovoltaic Specialist Conference, Denver, CO, USA, 8–13 June 2014; pp. 170–174.
44. Holmgren, W.F.; Groenendyk, D.G. An Open Source Solar Power Forecasting Tool Using PVLIB-Python. In Proceedings of the IEEE 43rd Photovoltaic Specialists Conference, Portland, OR, USA, 5–10 June 2016; pp. 972–975.
45. Stein, J.S. The Photovoltaic Performance Modeling Collaborative (PVPMC). In Proceedings of the 2012 38th IEEE Photovoltaic Specialists Conference, Austin, TX, USA, 3–8 June 2012; pp. 3048–3052.
46. Available online: https://ec.europa.eu/jrc/en/PVGIS/tools/tmy (accessed on 17 August 2018).
47. Andersen, F.M.; Baldini, M.; Hansen, L.G.; Jensen, C.L. Households' hourly electricity consumption and peak demand in Denmark. *Appl. Energy* **2017**, *208*, 607–619. [CrossRef]
48. Short, W.; Packey, D.; Holt, T. A Manual for the Economic Evaluation of Energy Efficiency and Renewable Energy Technologies. National Renewable Energy Laboratory—March 1995. Available online: https://www.nrel.gov/docs/legosti/old/5173.pdf (accessed on 20 January 2021).
49. Blejer, M.I.; Eden, B. A note on the specification of the fisher equation under inflation uncertainty. *Econ. Lett.* **1979**, *3*, 249–255. [CrossRef]
50. Dufo-López, R.; Cortés-Arcos, T.; Artal-Sevil, J.S.; Bernal-Agustín, J.L. Comparison of Lead-Acid and Li-Ion Batteries Lifetime Prediction Models in Stand-Alone Photovoltaic Systems. *Appl. Sci.* **2021**, *11*, 1099. [CrossRef]
51. Kost, C.; Shammugam, S.; Juelch, V.; Nguyen, H.; Schlegl, T. *Study: Levelized Cost of Electricity—Renewable Energy Technologies*; Fraunhofer ISE: Freiburg, Germany, 2018.
52. Newnham, R.H.; Baldsing, W.G.A. Benefits of partial-state-of-charge operation in remote-area power-supply systems. *J. Power Sources* **2002**, *107*, 273–279. [CrossRef]
53. de Vries, H.; Nguyen, T.T.; Veld, B.O.H. Increasing the cycle life of lithium ion cells by partial state of charge cycling. *Micrroelectronics Reliability* **2015**, *55*, 2247–2253. [CrossRef]
54. Wei, Z.; Zhao, J.; He, H.; Ding, G.; Cui, H.; Liu, L. Future smart battery and management: Advanced sensing from external to embedded multi-dimensional measurement. *J. Power Sources* **2021**, *489*, 229462. [CrossRef]